Chapter 1

Synthesis Strategies about 2D Materials

Jianghao Wang, Guangshe Li and Liping Li

Additional information is available at the end of the chapter

http://dx.doi.org/10.5772/63918

Abstract

In recent years, more and more attentions have been paid to two-dimensional (2D) materials due to the excellent electrical, optical, thermal and mechanical properties. To characterize the layer-dependent changes in properties and to provide pathways for their integration into a multitude of applications, it is essential to explore the reliable syntheses of single- and few-layer 2D materials. Therefore, many strategies, such as micromechanical exfoliation, ultrasonic exfoliation, hydrothermal method, topochemical transformation, chemical vapor deposition method and so on, have been developed to synthesize high-quality and ultrathin nanosheets showing their own merits and demerits in preparing 2D nanomaterials. Herein, an overview of the recent progress in the synthetic techniques is presented for 2D materials, in which we would introduce their experimental scheme, advantages and disadvantages, and applications of these synthetic strategies. Eventually, the potential trends and future directions for synthesizing technology for 2D materials are proposed.

Keywords: two-dimensional, nanosheets, top down, bottom up, synthesis strategy

1. Introduction

The discovery of single-layer graphene in 2004 by Novoselov and Geim has shown that it is highly possible to exfoliate stable, single-atom or single-polyhedral-thick two-dimensional (2D) materials from van der Waals solids, and these 2D materials could exhibit unique and fascinated physical properties, such as ultrahigh carrier mobility at room temperature (~10,000 $cm^2V^{-1}s^{-1}$), quantum hall effect, large theoretical specific surface area (2630 m^2g^{-1}), excellent optical transparency (~97.7%) and so on [1, 2]. This great discovery helps Novoselov and Geim win Nobel Prize in 2010. The success of graphene arouses intensive interests in 2D materials in the

world. As a consequence, more and more 2D materials have been synthesized successfully, showing great promise for in many applications.

Ideal 2D materials belong to those with only one atom or several atoms thickness and infinite lateral size. The reliable synthesis of single- and few-layer 2D materials is an essential first step for characterizing the layer-dependent changes in their properties, as well as for providing pathways of their integration into a multitude of applications [1]. For instances, when the thickness of metal Co was reduced to only one or several atoms, the catalytic activity of carbon dioxide reduction would be improved greatly when comparing to bulk metal Co [3]. Single-layer MoS_2 has been synthesized by mechanical exfoliation strategy and exhibits excellent performance in the field of gas sensors and phototransistors. It is worth noting that when bulk MoS_2 is exfoliated into monolayer, the type of band gap would change from indirect type to direct one [1, 4]. Another important example is that single-layered $Co(OH)_2$ can realize an ultrahigh energy density in all-solid-state asymmetric supercapacitor [5].

The emergence of these novel properties is the driving force for the rapid development of research in ultrathin 2D nanosheets, which has been on the forefront of scientific disciplines including chemistry, physics, materials, science, medicine and biology. However, the quest for methods of producing 2D materials with controlled thickness and lateral size has been always a challenging subject. This may be caused by the anisotropic crystal growth and strong chemical bonds in crystal structure. The common classification of crystalline structures according to the type of chemical bonds could be divided into van der Waals solids, layered ionic solids and nonlayered materials [1]. Every synthetic strategy has its own merits and demerits in preparing different kind of materials. Therefore, in this chapter, we concentrate on the different synthetic methods for synthesizing two-dimensional crystals. According to the principle of generating two-dimensional materials, we can divide the synthetic strategies into top-down and bottom-up strategies. The distinction between these two general classifications is based on the processes involved in the creation of the nanometer-sized structures [6]. In the bottom-up approach, nanoscale materials are constructed from atomic or molecular precursors that are allowed to react and grow in size or self-assemble into more complex structures. By contrast, the top-down approach carves nanoscale structures by controlled removal of materials from larger or bulk solids.

2. Top-down strategy

In top-down nanofabrication, the crafting of ultrathin nanosheets is achieved through physical-based or through chemical-based process. The physical top-down approach employs the use of mechanical force or ultrasonic wave to exfoliate layered van der Waals solids into single- and few-layer 2D materials, whereas the chemical top-down strategy relies essentially on chemical reaction that brought about by ion exchange or by the application of heat and so on. In this section, a brief overview is presented of the top-down synthetic process for 2D nanostructures, including their advantages and limitations.

2.1. Micromechanical exfoliation

Micromechanical exfoliation has been used to exfoliate graphite into single-layer graphene by Novoselov and Geim for the first time [2]. Mechanical exfoliation is a straightforward method to obtain only one- or few-layer nanosheets, which well maintains the crystal structure and properties. Beside this, versatility and low cost of this method make it highly popular for synthesizing 2D materials and extremely convenient for fundamental research. Even so, this method is limited to the laboratory research and seems impossible to scale up for industrial production. Although large size and high quality of ultrathin nanosheets can be obtained by this way, this method is applicable only for layered van der Waals solids. The nanosheets of layered ionic solids and nonlayered materials cannot be obtained by this strategy. Additionally, several other factors (stoichiometry and stacking orders) play the key roles in successful fabrication of monolayer MX_2 nanostructures by mechanical exfoliation. Herein, we take graphene as an example to introduce this method.

Graphene is a monolayer sheet of carbon, showing only one atom thickness but extending indefinitely in two dimensions, which is the typical representative of 2D materials. Many astonishing properties have been discovered for graphene, which include better electrical and thermal conductivity, mechanical strength and optical purity. The procedure of micromechanical exfoliation is very simple. **Figure 1** illustrates the process of mechanical exfoliation [7].

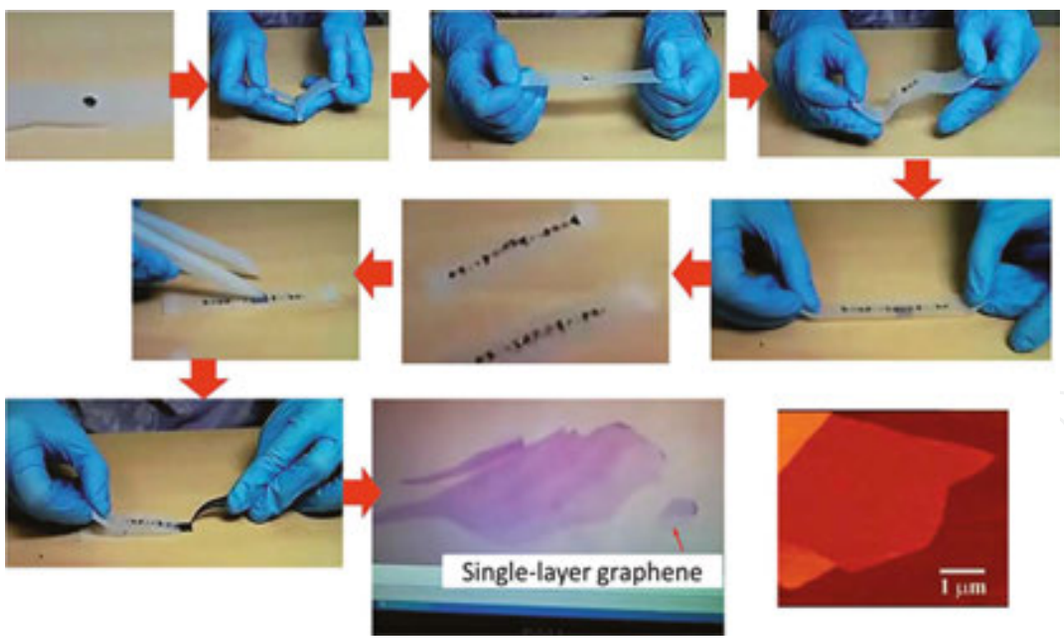

Figure 1. An illustrative procedure of the Scotch-tape–based micromechanical cleavage for graphene [7].

The exfoliation mechanics of this method are utilization of mechanical force to exfoliate graphite from Scotch tape. If one takes great pain to repeat this normal force over and over, the graphitic layer would become thinner and thinner, and eventually one can obtain single-layer graphene.

2.2. Ultrasonic exfoliation

Ultrasonic exfoliation is an effective strategy to delaminate van der Waals solids into single- or few-layer nanosheet. Compared to the mechanical exfoliation, this method is more effective and higher productive. The details for ultrasonic exfoliation process are shown in **Figure 2** [8]. As indicated in **Figure 2a**, sonication time and suitable solvents play the key roles in exfoliation. Suitable solvents are those with appropriate surface energies. In good solvents, the exfoliated nanosheets are stabilized against reaggregation. Otherwise, for "bad" solvents, reaggregation and sedimentation will occur. In recent reports, different types of organic solvents have been used as a dispersing medium for delaminating van der Waals solids (listed in **Table 1**) [8–14]. Although this method has many advantages, it is hard to get high-purity single-layer 2D material, which is a primary need for electronic applications. To make readers understand this method more in-depth, in the following, we will take black phosphorus (BP) as an example to introduce this strategy.

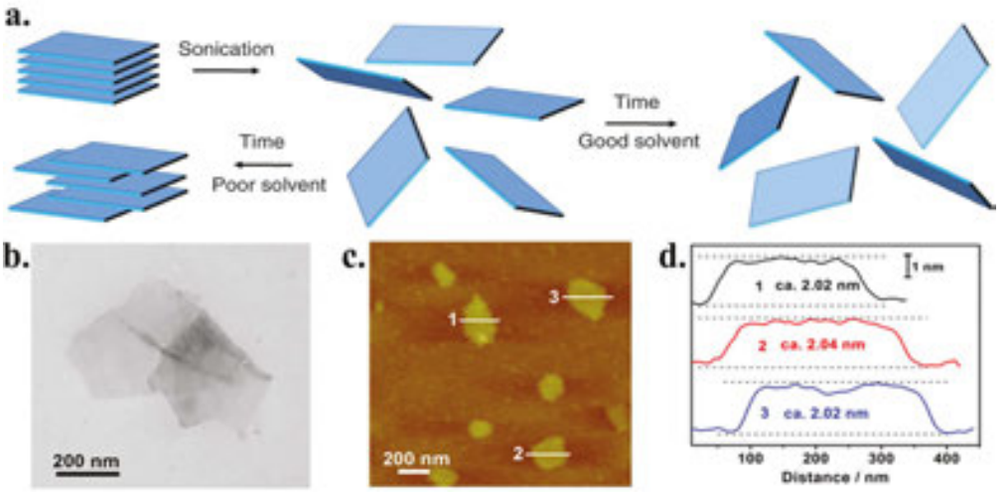

Figure 2. (a) An illustrative procedure of sonication-assisted exfoliation. The layered crystal is sonicated in a solvent, resulting in exfoliation and nanosheet formation [8]. (b) TEM image of ultrathin BP nanosheets. (c–d) AFM image and corresponding height image of ultrathin BP nanosheets [13].

	BN		**MoS_2**		**WS_2**	
	Solvent	**A/l (AU)[1] 300 nm**	**Solvent**	**A/l (AU) 670 nm**	**Solvent**	**A/l (AU) 630 nm**
1	Cyclohexylpyrrolidone (CHP)	100	NVP	100	DMSO	100
2	*N*-dodecyl-pyrrolidone (N12P)	61	N8P	98	NVP	92
3	Benzyl benzoate	44	N12P	97	NMF	90
4	Isopropanol	44	CHP	88	N12P	84
5	*N*-Octyl-pyrrolidone (N8P)	44	NMP	80	DMEU	75
6	*N*-vinylpyrrolidone (NVP)	41	DMEU	73	DMF	73

	BN		MoS_2		WS_2	
	Solvent	**A/l (AU)[1] 300 nm**	**Solvent**	**A/l (AU) 670 nm**	**Solvent**	**A/l (AU) 630 nm**
7	Benzyl $_e$ther	40	DMSO	61	Benzyl benzoate	71
8	Dimethyl-imidazolidinone (DMEU)	36	DMF	54	CHP	69
9	Cyclohexanone	29	DMA	54	Cyclohexanone	63
10	Chlorobenzene	28	Benzaldehyde	51	Benzonitrile	59
11	Dimethylsulphoxide (DMSO)	27	Benzonitrile	47	N8P	59
12	Benzonitrile	26	Benzyl benzoate	46	Isopropanol	59
13	Chlorobenzene	25	NMF	41	DMA	57
14	Chloroform	23	Cyclohexanone	38	Benzylether	55
15	Bromobenzene	23	Isopropanol	32	Chlorobenzene	45
16	*N*-Methyl-pyrrolidone(NMP)	23	Qunioline	26	Methanol	45
17	*N*-Methylformamide (NMF)	21	Acetone	24	Formamide	40
18	Dimethylformamide (DMF)	18	Benzylether	23	Bromobenzene	29
19	Dimethylacetamide (DMA)	16	Cyclohexane	22	Quinoline	26
20	Formamide	9	Methanol	21	Acetone	17

[1]A is absorbance; l is the path length of the beam of light through the material sample. A/l at fixed wavelength was used to estimate the mass remaining in the supernatant.

Table 1. The best 20 solvents for each material [9].

Single-layer BP is a very promising two-dimensional material that can be the substitution of graphene due to its exceptional electronic properties. The direct band gap of BP can be tuned from 0.3 eV in the bulk to 1.5 eV in the monolayer. Recently, Xie's group successfully prepared pristine 2D black phosphorus through direct ultrasonic exfoliation in organic solvent [13]. Briefly, they dispersed 50 mg of bulk black phosphorus in 100 mL of distilled water, which was bubbled with argon to eliminate the dissolved oxygen molecules for avoiding the oxidation. Then, sonicating the mixture solution in ice water for 8 h (Note: keeping the system at a relatively low temperature is important). After ultrasonic treatment, the resultant dispersions were centrifuged at 1500 rpm for 10 min to remove the unexfoliated component and the supernatant was collected for further use.

Ultrathin nanosheet thus obtained show lateral size of about several hundred nanometers (see TEM image in **Figure 2b**), and the ultrathin thickness is indicated by the near transparency of the sheets. AFM image and the corresponding height distribution (**Figure 2c** and **2d**) show that the measured height is about 2.0 nm, consistent with the four individual black phosphorus

layers. The black phosphorus nanosheets show excellent photodegradation of organic components such as DPBF and MO.

2.3. Lithium-intercalated and exfoliation

Ultrasonic exfoliation is incapable of peeling off a single layer of 2D nanostructure; herein, lithium (Li) intercalation process is introduced for synthesizing single sheets. The scheme of lithium-intercalated exfoliation strategy is shown in **Figure 3a** [15]. The formation of Li_xXS_2 compound is a key step in lithium intercalation process, and this reaction can be tuned to control the yield of single layers [16, 17]. The yield of this strategy for obtaining single-layer transition metal dichalcogenide is nearly 100%, while some challenges still remain. The first one is that the experiment is carried out at high temperature for long durations. Also, the lithium intercalation must be controlled carefully to obtain single-layer nanosheets, while preventing the formation of metal nanoparticles and precipitation of Li_2S. To make readers understand this method more in-depth, in the following, we would take MoS_2 as an example to introduce this strategy.

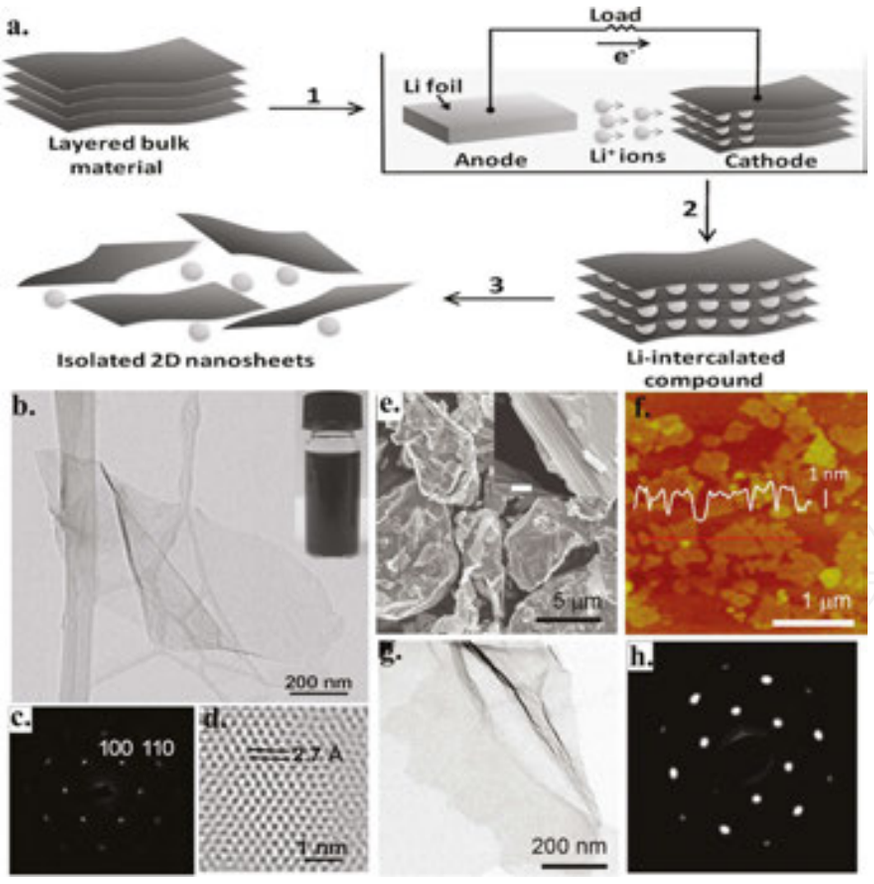

Figure 3. (a) Electrochemical lithiation process for the fabrication of 2D nanosheets from the layered bulk material. (b–d) Morphology characterization of MoS_2 exfoliated by electrochemical lithium-intercalated and exfoliation process [15]. (e–h) Morphology characterization of MoS_2 exfoliated by lithium-intercalated exfoliation process. [18].

2.3.1. Ultrathin nanosheets of MoS_2 through electrochemical lithium-intercalated exfoliation process

To control the step of the formation of $LixMoS_2$ compound, Zhang's group developed a simple method—electrochemical lithiation process—to control Li-intercalated and subsequent exfoliation in water or ethanol [15]. Lithium intercalation of MoS_2 is performed in a test cell. The bulk MoS_2 is prepared as cathode. The electrochemical intercalation is performed using galvanostatic discharge at a current density of 0.05 mA. After the discharge process, the product is washed with acetone to remove any residual electrolyte, followed by exfoliation and ultrasonication in distilled water or ethanol. Eventually, the suspension is centrifuged and washed many times with water.

As shown in **Figure 3b–d**, high-quality and ultrathin MoS_2 nanosheets can be obtained by this simple method. The lateral size of nanosheets is about several hundred nanometers with a near transparency. Electron diffraction pattern of a flat area of the nanosheet (**Figure 3c**) and the corresponding high-resolution transmission electron microscope (HRTEM) image (**Figure 3d**) show that the hexagonal lattice structure is formed by this method, showing clearly a lattice spacing of 2.7 Å assigned to the (100) planes. This strategy can also been applied to prepare other single-layer semiconducting nanosheets, such as WS_2, TiS_2, TaS_2 or graphene.

2.3.2. Ultrathin nanosheets of MoS_2 through lithium-intercalated exfoliation

Recently, Chhowalla's group successfully prepared monolayer MoS_2 through lithium-intercalated and exfoliation [18]. In detail, they immersed 3 g bulk MoS_2 crystals in certain concentration of butyllithium solution in hexane for 2 days in a flask filled with argon gas to obtain lithium intercalation compound. Exfoliation is achieved immediately after this process (within 30 min to avoid deintercalation) by ultra-sonicating Li_xMoS_2 in water for 1 h. The mixture is centrifuged several times to remove excess lithium in the form of LiOH and unexfoliated material.

Commercial MoS_2 powder (**Figure 3e**) was used to prepare highly monodisperse monolayer MoS_2 nanosheets through Li intercalation and exfoliation. As shown in **Figure 3f** and **g**, the lateral size of product is 300~800 nm and the average thickness is about 1~1.2 nm, which is larger than the dimension of 0.65~0.7 nm reported for mechanically exfoliated MoS_2 monolayers. This discrepancy may be explained by surface corrugation due to the distortions and the presence of adsorbed or trapped molecules. The absence of any sheets below the thickness values and no evidence of step edges on the nanosheets surface suggest that they consist of monolayers. The selected area electron diffraction (SAED) patterns indicate hexagonal symmetry of the atomic arrangement and that individual sheets consist of a single-crystal domain (**Figure 3h**). All of the results undoubtedly confirm that MoS_2 with monolayer thickness has been successfully synthesized.

2.4. Ion-change exfoliation

Although the exfoliation strategy mentioned previously is convenient to delaminate van der Waals solids into ultrathin nanostructure, it is hard to exfoliate layered ionic solids such as $LiCoO_2$ or LDHs. This is because these ionic solids have strong ionic bonds in the layers. Ion-

change exfoliation is a normal method to get this kind of 2D materials [19–23]. The scheme of ion-change exfoliation is shown in **Figure 4a** [19]. In the next section, we will take $LiCoO_2$ and (Co^{2+}-Co^{3+})-LDHs as examples to illuminate this method [23, 24].

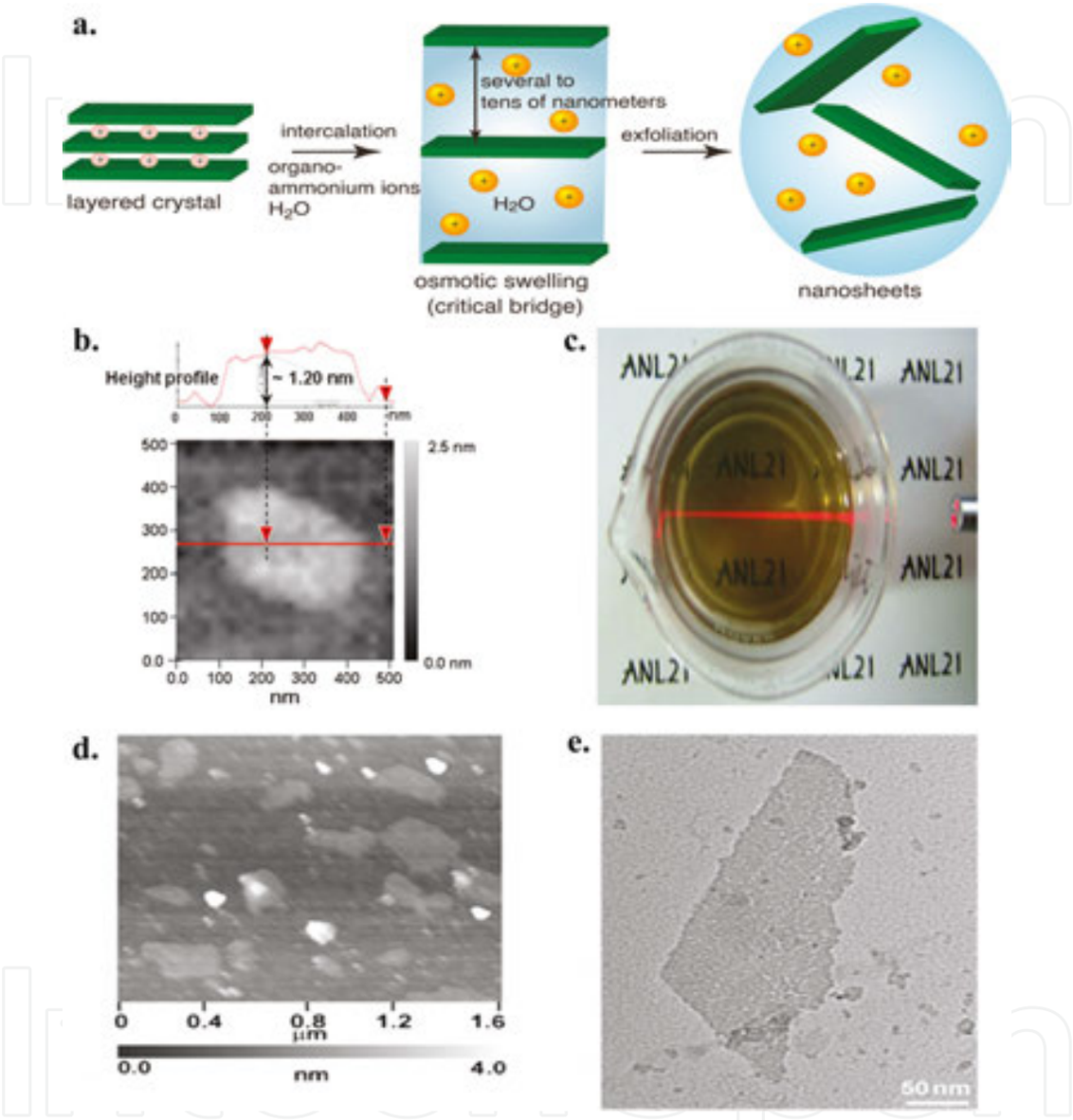

Figure 4. (a) Schematic illustration of the osmotic swelling to exfoliation process [19]. (b) AFM image and height profile of the exfoliated cobalt oxide adsorbed onto PEI-coated mica substrate. Photograph of the colloidal suspension of cobalt oxide. (c) The visible light is illuminated from the side of the beaker to demonstrate the Tyndall scattering effect [23]. Co^{2+}–Co^{3+} LDH nanosheets: (d) AFM image; (e) TEM image [24].

2.4.1. $LiCoO_2$

$LiCoO_2$ is a kind of cation-exchange layered metal oxides. Seong-Ju's group delaminated $LiCoO_2$ into monolayer recently [23]. The procedure of exfoliating could be described as follows: A proton-exchange reaction for the generation of layered $Li_xH_{1-x}CoO_2$ is carried out

in an aqueous solution of HCl (1 M, 1 mg mL^{-1} of $LiCoO_2$) at room temperature for 3 days. During the proton-exchange reaction, HCl solution is replaced with fresh solution every day. Exfoliation of the layered cobalt oxide is achieved by the intercalation of tetrabutylammonium (TBA) cation into the layers of $Li_xH_{1-x}CoO_2$. After the reaction, incompletely exfoliated particles were separated from the colloidal suspension through centrifugation (6000 rpm for 10 min), resulting in a pure colloidal suspension. The powdered samples of completely exfoliated nanosheets are collected from the pure colloidal suspension through high-speed centrifugation at 17,000 rpm for 30 min.

AFM of the as-obtained sample provides direct evidence for the exfoliation of layered cobalt oxide nanosheets (**Figure 4b**). The thickness of $LiCoO_2$ nanosheets is about 1.2 nm, which is slightly thicker than the crystallographic thickness of individual cobalt oxide layers. The observation of Tyndall phenomenon from the pure suspension, characteristic of colloidal suspensions, provides strong evidence for the exfoliation of layered cobalt oxide nanosheets too (**Figure 4c**).

2.4.2. (Co^{2+}-Co^{3+})-LDHs

According to Sasaki's report [24], 0.5 g of the sample is dispersed into an aqueous solution (500 mL) that contains 2.5 M $NaClO_4$ and 2.5 mM HCl. This mixed solution is carefully degassed by purging with nitrogen gas for conversion into ClO_4^--LDH (addition of HCl is crucial for preventing carbonate, CO_3^{2-} contamination from air). After purging with nitrogen gas, the reaction vessel is tightly capped and shaken for 1 day at room temperature. The sample is filtered, washed with degassed water and air-dried. The obtained ClO_4^- LDH (0.1 g) is mixed with formamide (100 mL) in a conical beaker. After an ultrasonic treatment for 30 min, a translucent colloidal suspension is obtained. The suspension is further centrifuged to remove possible nonexfoliated particles. AFM and TEM images shown in **Figure 4d** and **e** provided direct evidence for successfully exfoliation of the samples.

3. Bottom-up strategy

Top-down strategy is useful in preparing ultrathin and high-quality nanosheets with large lateral size. Even so, it has to be mentioned that all exfoliation methods as mentioned before are only suitable to those materials whose bulk crystals are layered [25]. The mass production by methods mentioned earlier is usually very low. When using bottom-up approach, nanoscale materials are constructed from atomic or molecular precursors that are suitable to react and grow in size, or self-assemble into more complex structures. Then, 2D materials can be enlarged easily [6]. In this section, a brief overview is presented for the bottom-up synthetic process to 2D nanostructures.

3.1. Wet chemical strategy

Wet chemical method is promising for preparing all types of 2D materials owing to its high-yield, low-cost and mass production. Wet chemical strategy is a big kind of synthesis method, which includes hydro/solvothermal synthesis and template synthesis. In this section, we introduce various types of wet-chemical synthesis strategies for preparing 2D nanomaterials.

3.1.1. Hydro/solvothermal synthesis

Hydro/solvothermal method is a common strategy used for the synthesis of inorganic materials. Advantages of hydro/solvothermal method over other types of crystal growth include low temperature (generally in a temperature range of 100–240°C) and convenience of adjusting reaction conditions. Many factors play the key roles in the synthesis of ultrathin nanostructure, which include temperature, reaction time, reactant ratio and so on. Many 2D materials have been prepared by this method, just like MoS_2, TiO_2, ZnO, Co_3O_4, MnO_2 and Rh [26–29]. In the following, we will take Li's work as an example to explain this strategy.

Ultrathin Rh nanosheets were synthesized successfully through solvothermal method by Li et al. recently [29]. For detailed steps, $Rh(acac)_3$ and PVP are dissolved in solvent mixed by benzyl alcohol and formaldehyde. The mixture is stirred vigorously for 1 h and then transferred to a Teflon-lined stainless steel autoclave. The autoclave is sealed and maintained at 180°C for 8 h and then cooled to room temperature. The resulted black product is precipitated with acetone (10 mL), separated in a centrifuge and washed three times with ethanol (10 mL) and finally dried under vacuum.

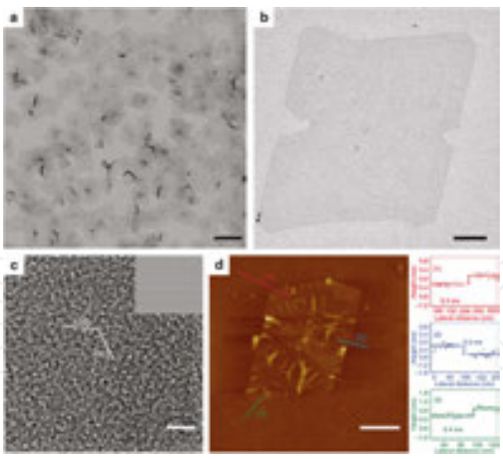

Figure 5. (a) Low-magnification TEM image of PVP-capped Rh nanosheet, (b) high-magnification TEM image of PVP-capped Rh NSs, (c) aberration-corrected microscopy image of PVP-capped Rh NS (inset, the corresponding filtered image using crystallographic average method to improve signal-to-noise ratio), (d) AFM image and the corresponding height profiles of a bare Rh NS [29].

Detailed structure information for the synthesized atomically thick Rh nanosheets is indicated by TEM, HRTEM and AFM. TEM image clearly shows that ultrathin nanosheet has a dimension lateral size of about 500 nm, while the near transparency of the sheets indicates the

ultrathin thickness (**Figure 5a, b**). As shown in **Figure 5c**, Rh nanosheets have a single crystalline nature of Rh nanosheets, which possesses a hexagonal structure, with a lattice parameter of ca. 2.6 Å, closer to the atomic distance of Rh (2.69 Å) in the (111) plane of the bulk Rh phase. AFM image of Rh NS shows that the sheet-like features are consistent with TEM images (see **Figure 5a**, **b**) Section analysis and height profile (**Figure 5d**) reveal that the height of Rh NS is about 4 Å. This is closer to the diameter of Rh atoms (the radius of Rh atomic is about 1.73 Å). All of these results undoubtedly confirm the successful synthesis of Rh nanosheets with an atomic thickness.

3.1.2. Template synthesis

A typical procedure of template method includes complicating morphology of template by growing crystal confined in specific dimension and then removing template through high temperature or adjusting pH. By this way, nearly all types of nanostructure including quantum dot (0D), nanowire (1D) and nanosheets (2D) can be prepared. The suitable template and condition of removing template are important. Many nonlayered structure 2D nanomaterials can be synthesized using the as-prepared 2D nanomaterials as the template, such as Fe_2O_3, Au, $CuInS_2$ and so on [30–32]. Herein, we take α-Fe_2O_3 as an example to illuminate this method.

3.1.2.1. Half-unit-cell thickness of alpha-Fe_2O_3 semiconductor nanosheets

Recently, Wei's group successfully synthesized free-standing half-unit-cell α-Fe_2O_3 nanosheets using CuO nanoplate as the template [30]. The layered iron hydroxide nanosheets are first prepared on CuO template surface by the mutually promoted slow interfacial reactions of Fe^{2+} hydrolysis and CuO-etching process at a low temperature of 25°C for a whole day, which

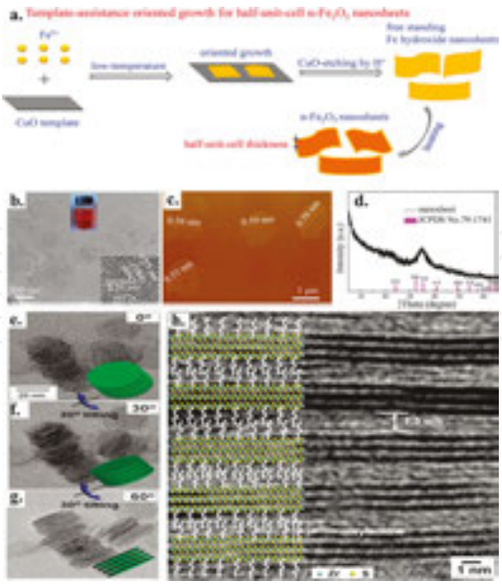

Figure 6. (a) Schematic of synthesis strategy of α-Fe_2O_3 nanosheets. (b) TEM image of the α-Fe_2O_3 nanosheets. The insets show the HRTEM image and the Tyndall effect of the α-Fe_2O_3 nanosheets. (c) AFM image and (d) XRD pattern of the α-Fe_2O_3 nanosheets [30]. (e–g) TEM images of the assembled ultrathin ZrS_2 nanodiscs obtained by rotating TEM holder under different angle. (h) HRTEM side-view image of multiply stacked 1.6-nm-thick ZrS_2 nanodiscs [33].

is beneficial for the synthesis of ultrathin nanosheets. When CuO template is etched out, a heat treatment is carried out for the dehydrogenation of Fe hydroxide nanosheets, which leads to the formation of the stable and free-standing α-Fe_2O_3 nanosheets.

AFM and TEM image provide direct evidence for successful exfoliation of the sample. As shown in **Figure 6b**, **c**, the lateral size of α-Fe_2O_3 nanosheets is up to about 1 μm, and thickness is about 0.55–0.59 nm. The XRD pattern of the α-Fe_2O_3 shown in **Figure 6d** exhibits only a broad and weak diffraction peak corresponding to the (110) orientation plane of α-Fe_2O_3. It is interesting to note that ultrathin α-Fe_2O_3 nanosheet shows an intrinsic ferromagnetism of 0.6 μ_B/atom at 100 K and remains ferromagnetism at room temperature.

3.1.2.2. Ultrathin zirconium disulfide nanodiscs

Except for hard template, soft colloidal templated synthesis is used to prepare two-dimensional2D materials frequently. The long-chain oleylamine and/or oleic acid surfactants are often used as the soft colloidal templates for directing the crystal growth. Cheon et al. used this method to synthesize ultrathin ZrS_2 nanodiscs [36]. Intermediate lamellar complexes composed of 2D arrays of $ZrCl_4$ and alkyl amine are first obtained, in which alkyl amine serves as the soft colloidal template. Then, CS_2 is injected into the mixture aforementioned to form ultrathin ZrS_2 nanodiscs dispersed in solution.

As indicated in **Figure 6e–h**, the resultant ultrathin ZrS_2 nanodiscs possess radius of ~15 nm and thickness of 0.5 nm. The spacing between the discs is ~1.5 nm (**Figure 6h**), which corresponds to the length of the oleylamine surfactant layers. When compared to bulk ZrS_2, ultrathin ZrS_2 discs show the unique nanoscale size effects, enhanced discharge capacity by 230% and greatly improved stability.

3.2. Microwave-assisted method

In recent years, microwave-assisted chemical synthesis strategy has become a well-established technique to promote and enhance chemical reactions. The main advantages of this method are represented by much shorter reaction time (generally in only a few minutes) and higher energy efficiency when comparing to other conventional strategies. Due to these advantages, some 2D nanomaterials can be prepared by this way conveniently, such as SnO_2, α-$Ni(OH)_2$, $K_{0.17}MnO_2$ and CuSe [33–37].

To understand it more clearly, let us take α-$Ni(OH)_2$ as an example (**Figure 7**) [36]: firstly, precursors were prepared by starting materials of $Ni(NO_3)_2{\cdot}6H_2O$, urea, deionized water and ethylene glycol at given proportions. Then, the resulting solution is transferred into a home-made round-bottomed flask and treated under microwave irradiation in a microwave reactor at 700 W for several minutes. Finally, the green powder is obtained by centrifugation and washed several times with distilled water and absolute ethanol. After that, the powder was dried in vacuum at 80°C for 12 h. Detailed structure information for the synthesized $Ni(OH)_2$ nanosheets is unraveled by FESEM and TEM images in **Figure 7b–d**. In comparison with traditional wet-chemical syntheses, the microwave-assisted liquid-phase growth can

shorten the reaction time to less than 20 min. Particularly, the ultrathin α-Ni(OH)$_2$ nanosheets exhibit a maximum specific capacitance of 4172.5 Fg^{-1} at a current density of 1 Ag^{-1}.

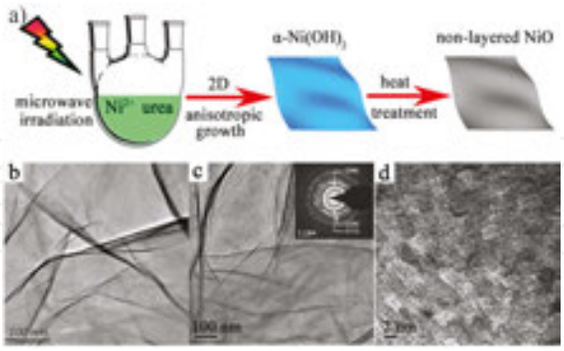

Figure 7. (a) Schematic illustration for the synthesis of nanosheets. (b) High magnification FESEM images of α-Ni(OH)$_2$ nanosheets, (c) TEM image (the inset showing SAED pattern) and (d) a planar HRTEM image [36].

3.3. Topochemical transformation

Topological conversion is a strategy in which the product's morphology is inherited from their precursor through nucleation and growth inside the precursors. The key to success is the degree of lattice match between precursor and their product. From the viewpoint of anisotropy of layered compounds, it is easier to obtain 2D nanostructure of hydroxide rather than oxides. This method is applicable of preparing nonlayer 2D nanostructure oxides, such as Co_3O_4, CeO_2 and δ-FeOOH [38–40]. In the following, we will take Co_3O_4 and Ni as examples to illuminate this method [38, 41].

3.3.1. Atomically thick Co_3O_4 nanosheets through topotactic oxidation transformation

The schematic illustration of the preparation of ultrathin Co_3O_4 nanosheets is shown in **Figure 8**. As illustrated in **Figure 8a**, the thickness of (001)-oriented few layered α-Co(OH)$_2$ is

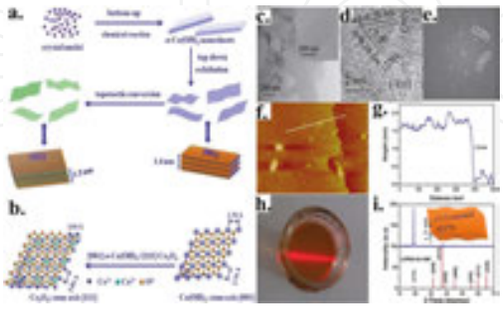

Figure 8. (a) Schematic illustration of the preparation of ATCNs. (b) Schematic model of the top-view illustrating the topochemical transformation from α-Co(OH)$_2$ (001) plane to Co_3O_4 (111) plane. (c–e) TEM image, HRTEM image and the corresponding fast Fourier transform pattern of ATCNs. (f and g) Tapping model AFM image and corresponding height profile of as-obtained nanosheets deposited on a silicon substrate. (h) Photograph of a colloidal suspension of the ATCNs displaying the Tyndall effect. (i) XRD pattern of ATCNs-based film displaying highly preferred [111] orientation [38].

closer to the thickness of (111)-oriented Co_3O_4 nanosheets. More specifically, the discrepancies between α-$Co(OH)_2$ {100} (d=2.76 Å) and Co_3O_4 {220} (d=2.84 Å) are calculated to be below 3%. Moreover, Co^{2+} atomic arrangement in α-$Co(OH)_2$ (001) plane and Co_3O_4 (111) plane is very closer (**Figure 8b**). These features enable atomically thick Co_3O_4 nanosheets to preserve the thickness of the precursor possible.

Atomically thick Co_3O_4 nanosheets were prepared by this method, as confirmed by TEM, AMF and XRD. From TEM image, one could clearly see ultrathin nanosheets with lateral size of about 400 nm with the near transparency of the sheets (**Figure 8c**). HRTEM image, and the corresponding fast Fourier transform (FFT) pattern in **Figure 8d** and **e** for the as-obtained product depicts its [111] preferential orientation. The thickness of the as-synthesized Co_3O_4 nanosheets is also evaluated by tapping-mode atomic force microscopy (AFM). AFM image and the corresponding height distribution (**Figure 8f, g**) show that the measured height is about 1.5 nm. Microscopically, the colloidal suspension of the product displays the Tyndall phenomenon (**Figure 8h**), so that the formation of homogeneous ultrathin nanosheets in ethanol can be inferred. As shown in **Figure 8i**, XRD pattern of the atomically thick nanosheet-based films can be readily indexed to be pure Co_3O_4 (JCPDS no. 42-1467) and also displays the highly preferred [111] orientation, which is corresponding to the result of HRTEM. All of the results undoubtedly confirm that Co_3O_4 nanosheets with ultrathin thickness have been successfully synthesized. The oriented growth of ATCNs is attributed to α-$Co(OH)_2$-to-Co_3O_4 topochemical conversion with the relationship of [001] α-$Co(OH)_2$ and [111] Co_3O_4.

3.3.2. Ultrathin nickel nanosheets through topotactic reduction transformation

Except for topotactic oxidation, toporeduction is also frequently used to prepare nonlayered materials. Sun [41] used this method and synthesized ultrathin nickel nanosheets array recently. $Ni(OH)_2$ nanosheet array on a metal substrate is prepared first. And then, ethylene glycol is used as the reduction agent to get Ni nanosheets. The slow conversion kinetics keeps the ultrathin nanosheet morphology and atomic thickness.

Figure 9 reveals the morphology inherence between Ni and $Ni(OH)_2$ nanosheet array. **Figure 9a**, **b** shows SEM and HRTEM of $Ni(OH)_2$ sheet array. It is seen that the thickness of $Ni(OH)_2$ is about 5.8 nm (10–12 layers), whereas the thickness of Ni nanosheet shown in

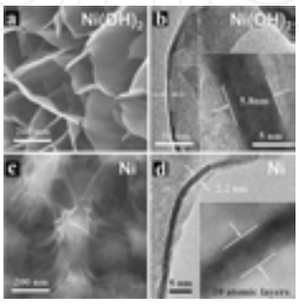

Figure 9. (a and c) SEM images of the as-synthesized $Ni(OH)_2$ nanowall array and Ni-NSA. (b and d) HRTEM image of a scrolled $Ni(OH)_2$ nanowall and a vertically laid Ni nanosheet. The inset shows the thickness of $Ni(OH)_2$ nanowall and Ni nanosheet [41].

Figure 9c, **d** is about 2.2 nm (10 atomic layers). This provides strong evidence that Ni nanosheets are obtained by toporeduction transformation.

3.4. Chemical vapor deposition (CVD)

Recently, CVD technique has shown promise to generate high-quality TMD layers with a scalable size, controllable thickness and excellent electronic properties. CVD is a high-temperature chemical synthesis process by which a desired material is deposited on substrates. CVD processes have been extensively studied for synthesizing thin film coatings of a wide range of materials, including metals, semiconductors, and insulators. The scheme of CVD method is shown in **Figure 10a** [1]. The precursor vapor is introduced from outside or generated inside the tube furnace. The main advantages of CVD synthesis process are represented by the accesses to high quality, high purity 2D nanomaterials with controlled properties, which allow one to control the morphology, crystallinity and defects of 2D nanostructures by tuning the process parameters [42]. Due to these advantages, some 2D nanomaterals have been prepared by this way conveniently, such as graphene, MoS_2, h-BN [43–49]. CVD method is also another annealing strategy for the growth of high-quality single-crystalline 2D sheet on substrates. Even so, CVD suffers from the requirement of high temperature, high vacuum and specific substrates. In the following, we will take h-BN and MoS_2 as an example to elaborate this strategy.

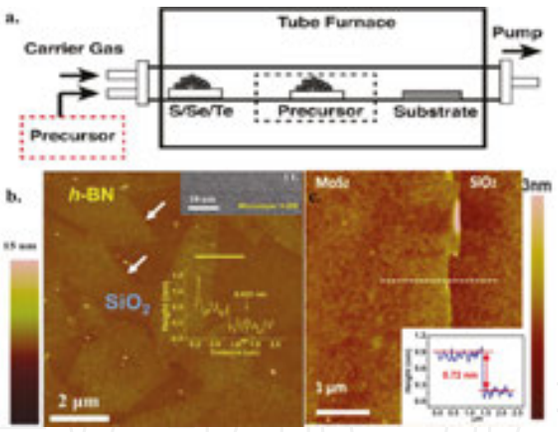

Figure 10. (a) Schematic illustration of experimental setup for the 2D materials synthesis by a noncatalytic vapor deposition process. The precursor vapor can be introduced from outside or generated inside the tube furnace [1]. (b) AFM images of the initial flakes of h-BN. White arrows point to the sharp edges of these flakes. Inset: TEM image of the folded edge of a monolayer h-BN [43]. (c) AFM image of a monolayer MoS_2 film on a SiO_2/Si substrate. Inset: corresponding height profile of as-obtained nanosheets [46].

Hexagonal BN is called "white graphite" due to its similar lamellar structure to graphite. h-BN possesses many unique properties such as chemical stability, strong mechanical strength, high-thermal conductivity and low dielectric constant. What is more, the band gap of h-BN can be tuned with thickness. To produce BN precursor, the first heating zone is ramped up to T_1=60∼90°C with a heating belt. Turn on the on-off valve between the first and second heating zone only during CVD process, one can prevent the undesired growth. The second heating

zone is heated up to T_2 = 1000°C for typically 10~90 min under 10 sccm hydrogen atmosphere at a pressure of 350 mTorr after mounting the copper foil. Copper foil (25 μm, Alfa Aesar) is used as the metal catalyst substrate. Before the growth of h-BN, copper foil is annealed at 1000°C for 20 min under 10 sccm H_2 to grow the copper grain and to obtain a smooth surface. AFM of as-obtained sample provides direct evidence for single-layer h-BN synthesized by chemical vapor deposition method (**Figure 10b**). AFM image and the corresponding height distribution inset in **Figure 10b** show that the measured height is about 0.42 nm, consistent with monolayer thickness (c-axis spacing for h-BN is ~0.32 nm). In addition, TEM image of monolayer h-BN clearly demonstrates that the number of layer of h-BN is one (**Figure 10c**). Moreover, for a complete h-BN layer (**Figure 10d**), the wrinkles of h-BN film (indicated by a yellow arrow) under scanning electron microscopy (SEM) can be clearly seen. These wrinkles are characteristic of h-BN and graphene films due to the negative thermal expansion coefficients of h-BN and graphene. All of the results undoubtedly confirm that h-BN with monolayer thickness have been successfully synthesized.

Synthesis of transition metal dichalcogenides (TMDs) using CVD is the cutting edge research area in recent years. Lee [46] synthesized single-layer MoS_2 by this method recently. As shown in **Figure 10c**, ultrathin MoS_2 nanosheets with smooth surface are observed with AFM. The cross-sectional height in inset of **Figure 10c** reveals that the thickness of MoS_2 film is ~0.72 nm, which corresponds to a monolayer MoS_2.

4. Perspective and conclusions

With the advantages of very high surface-to-volume ratios and special electronic properties in two-dimensional materials, ultrathin nanosheets are very promising in catalysis, supercapacitors, photoconductive materials, batteries and magneto-optical components. Therefore, it is imperative to exploit more technologically advanced synthesis strategies to obtain high quality, large size, ultrathin two-dimensional materials. At present, thinner, larger size, high productive and quality nanosheets are still the chief purpose for scientists. Usually, the thinner nanosheets give a higher catalytic performance and other special properties. Besides these, controllable thickness, architectures assembled by nanosheets and composite nanostructure, such as quantum-dot/nanosheets, sandwich structure and modification on two-dimensional nanosheets, also provide new opportunities for material science.

In summary, synthetic strategies, such as top-down and bottom-up method, have been employed for synthesizing two-dimensional crystals. The top-down strategy includes micromechanical exfoliation, ultrasonic exfoliation, lithium-intercalated and exfoliation and ion-change exfoliation. Using top-down strategies, one is able to obtain high-quality and large-size two-dimensional crystal conveniently. Even so, this method is only appropriate for those materials whose bulk crystals are layered. Comparatively, bottom-up strategy could overcome this shortage. Bottom-up strategy is composed of wet chemical method, microwave-assisted chemical, topological conversion strategy and chemical vapor deposition method. All these strategies may present different features and questions for preparing two-dimensional

materials. In the future, scientists should take more and more efforts to develop new synthetic technologies for high-quality 2D material and the relevant applications.

Author details

Jianghao Wang[1], Guangshe Li[2] and Liping Li[1*]

*Address all correspondence to: Lipingli@fjirsm.ac.cn

1 Key Laboratory of Design and Assembly of Functional Nanostructures, Fujian Institute of Research on the Structure of Matter, Fuzhou, P.R. China

2 State Key Laboratory of Inorganic Synthesis and Preparative Chemistry, College of Chemistry, Jilin University, Changchun, P.R. China

References

[1] Joshua EG. Progress, challenges, and opportunities in two-dimensional materials beyond graphene. ACS Nano. 2014;7(4): 2898–2962. DOI: 10.1021/nn400280c

[2] Novoselov KS. Electric field effect in atomically electric field effect in atomically. Science. 2004;306(5696): 666–669. DOI: 10.1126/science.1102896

[3] Xie Y. Partially oxidized atomic cobalt layers for carbon dioxide electroreduction to liquid fuel. Nature. 2016;529(7484): 68–71. DOI: 10.1038/nature16455

[4] Zhang H. Single-layer MoS2 phototransistors. ACS Nano. 2012;6(1): 74–80. DOI: 10.1021/nn2024557

[5] Gao S. Ultrahigh energy density realized by a single-layer beta-Co(OH)2 all-solid-state asymmetric supercapacitor. Angew Chem Int Ed Engl. 2014;53(47): 12789–12793. DOI: 10.1002/anie.201407836

[6] Han MY. Chemical routes to top-down nanofabrication. Chem Soc Rev. 2013;42(14): 6006–6018. DOI: 10.1039/c3cs60113g

[7] Shen ZG. A review on mechanical exfoliation for the scalable production of graphene. J. Mater. Chem. A. 2015;3(22):11700–11715. DOI: 10.1039/c5ta00252d

[8] Coleman JN. Liquid exfoliation of layered materials. Science. 2013;334(6052): 72–75. DOI: 10.1126/science.1208891

[9] Coleman JN. Two-dimensional nanosheets produced by liquid exfoliation of layered materials. Science. 2011;331(6017): 568–571. DOI: 10.1126/science.1194975

[10] Coleman JN. Large-scale exfoliation of inorganic layered compounds in aqueous surfactant solutions. Adv Mater. 2011;23(34): 3944–3948. DOI: 10.1002/adma.201102584

[11] Zhang HL. A Mixed-solvent strategy for efficient exfoliation of inorganic graphene analogues. Angew Chem Int Ed Engl. 2011;50(46): 10839–10842. DOI: 10.1002/anie.201105364

[12] Coleman JN. Preparation of high concentration dispersions of exfoliated MoS2 with increased flake size. Chem Mater. 2012;24(12): 2414–2421. DOI: 10.1021/Cm301515z

[13] Xie Y. Ultrathin black phosphorus nanosheets for efficient singlet oxygen generation. J Am Chem Soc. 2015;137(35): 11376–11382. DOI: 10.1021/jacs.5b06025

[14] Hersam MC. Solvent exfoliation of electronic-grade, two-dimensional black phosphorus. ACS Nano. 2015;9(4):3596–3604. DOI: 10.1021/acsnano.5b01143

[15] Zhang H. Single-layer semiconducting nanosheets: high-yield preparation and device fabrication. Angewandte Chemie. 2011;50(47): 11093–11097. DOI: 10.1002/anie.201106004

[16] Zhang H. The chemistry of two-dimensional layered transition metal dichalcogenide nanosheets. Nat Chem. 2013;5(4): 263–275. DOI: 10.1038/nchem.1589

[17] Chen M. Chemically exfoliated ReS2 nanosheets. Nanoscale. 2014;6(21): 12458–12462. DOI: 10.1039/c4nr03740e

[18] Chhowalla M. Photoluminescence from chemically exfoliated MoS2. Nano Lett. 2011;11(12): 5111–5116. DOI: 10.1021/nl201874w

[19] Sasaki T. Two-dimensional oxide and hydroxide nanosheets: controllable high-quality exfoliation, molecular assembly, and exploration of functionality. Acc Chem Res. 2014;48(1): 136–143. DOI: 10.1021/ar500311w

[20] Hwang SJ. Composition-tailored 2 D Mn(1-x)Ru(x)O(2) nanosheets and their reassembled nanocomposites: improvement of electrode performance upon Ru substitution. Chem Eur J. 2014;20(17): 5132–5140. DOI: 10.1002/chem.201304009

[21] Sasaki T. Exfoliated oxide nanosheets: new solution to nanoelectronics. J Mater Chem. 2009;19(17): 2503. DOI: 10.1039/b820160a

[22] Sasaki T. Osmotic swelling to exfoliation. Exceptionally high degrees of hydration of a layered titanate. J Am Chem Soc. 1998;120(19): 4682–4689. DOI: 10.1021/Ja974262l

[23] Hwang SJ. Soft-chemical exfoliation route to layered cobalt oxide monolayers and its application for film deposition and nanoparticle synthesis. Chem Eur J. 2009;15(41): 10752–10761. DOI: 10.1002/chem.200901590

[24] Sasaki T. Topochemical synthesis of monometallic (Co2+-Co3+) layered double hydroxide and its exfoliation into positively charged Co(OH)2 nanosheets. Angew Chem Int Ed Engl. 2008;47(1): 86–89. DOI: 10.1002/anie.200703941

[25] Zhang H. Wet-chemical synthesis and applications of non-layer structured two-dimensional nanomaterials. Nat Commun. 2015;6:7873. DOI: 10.1038/ncomms8873

[26] Xue JM. Ultrasmall Fe3O4 nanoparticle/MoS2 nanosheet composites with superior performances for lithium ion batteries. Small. 2014;10(8): 1536–1543. DOI: 10.1002/smll.201302879

[27] Bai H. Large-scale, ultrathin and (001) facet exposed TiO2 nanosheet superstructures and their applications in photocatalysis. J Mater Chem A. 2014;2(7): 2040. DOI: 10.1039/c3ta14343k

[28] Dou SX. Generalized self-assembly of scalable two-dimensional transition metal oxide nanosheets. Nat Commun. 2014;5: 3813. DOI: 10.1038/ncomms4813

[29] Li J. Ultrathin rhodium nanosheets. Nat Commun. 2014;5: 3039. DOI: 10.1038/ncomms4093

[30] Wei S. Half-unit-cell alpha-Fe2O3 semiconductor nanosheets with intrinsic and robust ferromagnetism. J Am Chem Soc. 2014;136(29): 10393–10398. DOI: 10.1021/ja504088n

[31] Zhang H. Synthesis of hexagonal close-packed gold nanostructures. Nat Commun. 2011;2: 292. DOI: 10.1038/ncomms1291

[32] Xie Y. CuInSe2 ultrathin nanoplatelets: novel self-sacrificial template-directed synthesis and application for flexible photodetectors. Chem Commun. 2012;48(73): 9162–9164. DOI: 10.1039/c2cc34727j

[33] Xie Y. Ultra-rapid microwave-assisted synthesis of layered ultrathin birnessite K0.17MnO2 nanosheets for efficient energy storage. J Mater Chem A. 2013;1(28): 8154–8159. DOI: 10.1039/C3ta11194f

[34] Cheon J. Ultrathin zirconium disulfide nanodiscs. J Am Chem Soc. 2011;133(20): 7636–7639. DOI: 10.1021/ja200400n

[35] Cao C. Microwave-assisted and gram-scale synthesis of ultrathin SnO2 nanosheets with enhanced lithium storage properties. ACS Appl Mater Interfaces. 2015;7(4):2745–2753. DOI: 10.1021/am507826d

[36] Li YD. Ultrathin nickel hydroxide and oxide nanosheets: synthesis, characterizations and excellent supercapacitor performances. Sci Rep. 2014;4:5787. DOI: 10.1038/srep05787

[37] Pan GB. Facile microwave-assisted synthesis of Klockmannite CuSe nanosheets and their exceptional electrical properties. Sci Rep. 2014;4:5998. DOI: 10.1038/srep05998

[38] Xie Y. Topochemical transformation route to atomically thick Co3O4 nanosheets realizing enhanced lithium storage performance. Nanoscale. 2013;5(12):5241–5246. DOI: 10.1039/c3nr01178j

[39] Sun Y. Pits confined in ultrathin cerium (IV) oxide for studying catalytic centers in carbon monoxide oxidation. Nat Commun. 2013;4:2899. DOI: 10.1038/ncomms3899

[40] Chen PZ. Ultrathin nanosheets of feroxyhyte: a new two-dimensional material with robust ferromagnetic behavior. Chem Sci. 2014;5(6):2251. DOI: 10.1039/c3sc53303d

[41] Sun X. Single-crystalline ultrathin nickel nanosheets array from in situ topotactic reduction for active and stable electrocatalysis. Angew Chem Int Ed Engl. 2016;55(2): 693–697. DOI: 10.1002/anie.201509616

[42] Li LJ. Recent advances in controlled synthesis of two-dimensional transition metal dichalcogenides via vapour deposition techniques. Chem Soc Rev. 2014;DOI: 10.1039/c4cs00256c

[43] Kong J. Synthesis of monolayer hexagonal boron nitride on Cu foil using chemical vapor deposition. Nano Lett. 2012;12(1):161–166. DOI: 10.1021/nl203249a

[44] Rodney SR. Large-area synthesis of high-quality and uniform graphene films on copper foils. Science. 2009;324(5932):1312–1314. DOI: 10.1126/science.117124

[45] Kong J. Role of the seeding promoter in MoS2 growth by chemical vapor deposition. ACS Nano. 2014;14(2):464–472. DOI: 10.1021/nl4033704

[46] Lee YH. Synthesis of large-area MoS2 atomic layers with chemical vapor deposition. Adv Mater. 2012;24(17):2320–2325. DOI: 10.1002/adma.201104798

[47] Nayak PK. Robust room temperature valley polarization in monolayer and bilayer WS2. Nanoscale. 2016;8:6035–6042. DOI: 10.1039/C5NR08395H

[48] Shaw JC. Chemical vapor deposition growth of monolayer MoSe2 nanosheets. Nano Res. 2014;7(4):511–517. DOI: 10.1007/s12274-014-0417-z

[49] Huang JK. Large-area synthesis of highly crystalline WSe2 monolayers and device applications. ACS Nano. 2014;8(1):923–930. DOI: 10.1021/nn405719x